Single Photon Emission from Rewritable Nanoimprinted Localized Emitter Arrays in Atomically Thin Crystals

Ying-Yu Lai,[†,‡] *Po-Han Chen,*[‡] *Chun-An Chen,*[‡] *Yi-Hsien Lee,*[‡] *and Hui Deng* ***,**[†]

[†]Department of Physics, University of Michigan, Ann Arbor, MI 48109, USA

[‡]Materials Science and Engineering, National Tsing-Hua University, Hsinchu 20013, Taiwan

Abstract

Atomically thin van der Waals crystals have emerged as a new class of single photon emitters (SPEs) that can be created and controlled by strain engineering. Transferring monolayer (ML) crystals over nanostructures enabled position-controlled arrays of SPEs, but the process is hard to control, has low yield. Pressing a ML with Atomic Force Microscope tips allows greater control but is slow and expensive. Here we show that nanoimprint on atomically thin crystals provides a new route to rapid creation of large, rewritable arrays of localized emitters with high yield. Bright and narrow emission is observed from >90% of the imprinted nanoholes in monolayer tungsten diselenide (WSe_2). The emission features anti-bunching and persists up to 150 K. We furthermore demonstrate erasing and rewriting of the emitter arrays, which enables greater flexibility. SPEs created by the nanoimprint method will be compatible with integration with micro-/nano-photonic structures, and the method can be applied to a wide range of 2D materials and their heterostructures.

KEYWORDS : Nanoimprint, single photon emitter, two dimensional semiconductor, tungsten diselenide

Main

Solid-state non-classical light emitters are at the heart of many quantum information technologies such as cryptography, communication, and metrology.[1] Tremendous progress has been made on a variety of single-photon emitters (SPEs) in the past few decades.[2-7] However, limitations in the positioning, scalability, integration, and operating wavelength and temperature have hampered their applications. Recently, two-dimensional (2D) semiconductors, such as transition metal dichalcogenides (TMDs),[8-12] GaSe,[13] and hBN,[14] have been discovered as a new type of single-photon source that may overcome these limitations.[15] They can operate at higher temperatures due to strong exciton binding. The exciton wavelength ranges from visible to near infrared in different TMDs. Most importantly, as van der Waals materials, they allow controlled fabrication and integration with diverse material platforms.

When monolayer TMDs are placed over a substrate with protruding nanopillars or indented nanoholes, strain introduced by the nanostructures has led to single photon emission from defect-bound excitons at these positions.[16-18] This provides a route to position-controlled single photon source via strain engineering[18-27] However, since the deformation of the 2D crystals formed around the nanostructures is non-conformal, it is difficult to predict or control the resulting strain potential and SPE properties. Protruding nanostructures also pose a risk to pierce the 2D crystals, limiting the creation yield of the SPEs. Furthermore, the nanostructured substrate makes it difficult to integrate the SPE with commonly used photonic structures, such as photonic crystal cavities and waveguides, which are necessary for efficient coupling with the single photons and further on-chip integration. Alternatively, it was shown that a more controllable and repeatable strain profile can be created by stressing the monolayers using an Atomic Force Microscope (AFM) tip.[28] Yet the method is expensive, slow, and limited to small areas.

In this work, we demonstrate a nanoimprint-based method for low-cost, rapid creation of large arrays of localized emitters, with high yield and controlled strain morphology. Nanoimprint[29] has been widely used with conventional materials to create sub-micron photonic structures, for it is flexible, scalable and cost-effective. Here we demonstrate for the first time using nanoimprint to create quantum emitters, in atomically thin crystals. This method of creating SPEs is scalable and compatible with further on-chip integration of nano-photonic structures.

We use a SiO_2 nanorod array as an imprinting mold to strain a WSe_2 ML on a PET film with a nanohole morphology, so as to localize the defect-bound exciton in the nanohole region. Figure 1a~1c shows the schematic of the nanoimprint process. The principle is similar to that of the thermal imprint lithography, where a nanostructure pattern is created in an etch mask by pressing a mold onto the mask at elevated temperatures. [29] Here a ML crystal is placed on a polyester (PET) stamp and pressed onto the mold. When the mold temperature is raised to above the glass transition temperature of the polymer, the PET and ML crystal together conform to the morphology of the mold, and the nanostructure pattern of the mold is imprinted onto the ML crystals. After imprinting, the temperature is lowed to the room temperature and the strained ML crystal is delaminated from the mold while retaining the nanostructure morphology (see Methods for details of the process).

We first confirm the imprinting using an optical microscope under microscope light source, as shown in Figure 1d. The region in the yellow frame depicts the monolayer WSe_2. The imprinted nanoholes are visible as darker scattering centers. To compare the imprinted nanoholes with the nanorod mold, we perform AFM scans on both. The AFM images of the nanorod (Fig. 1e) and nanohole arrays (Fig. 1f) show the same array structure, with the same period of 4 μm. In Fig. 1g, we compare the inverted height line-scan across a nanorod and the depth line-scan across a

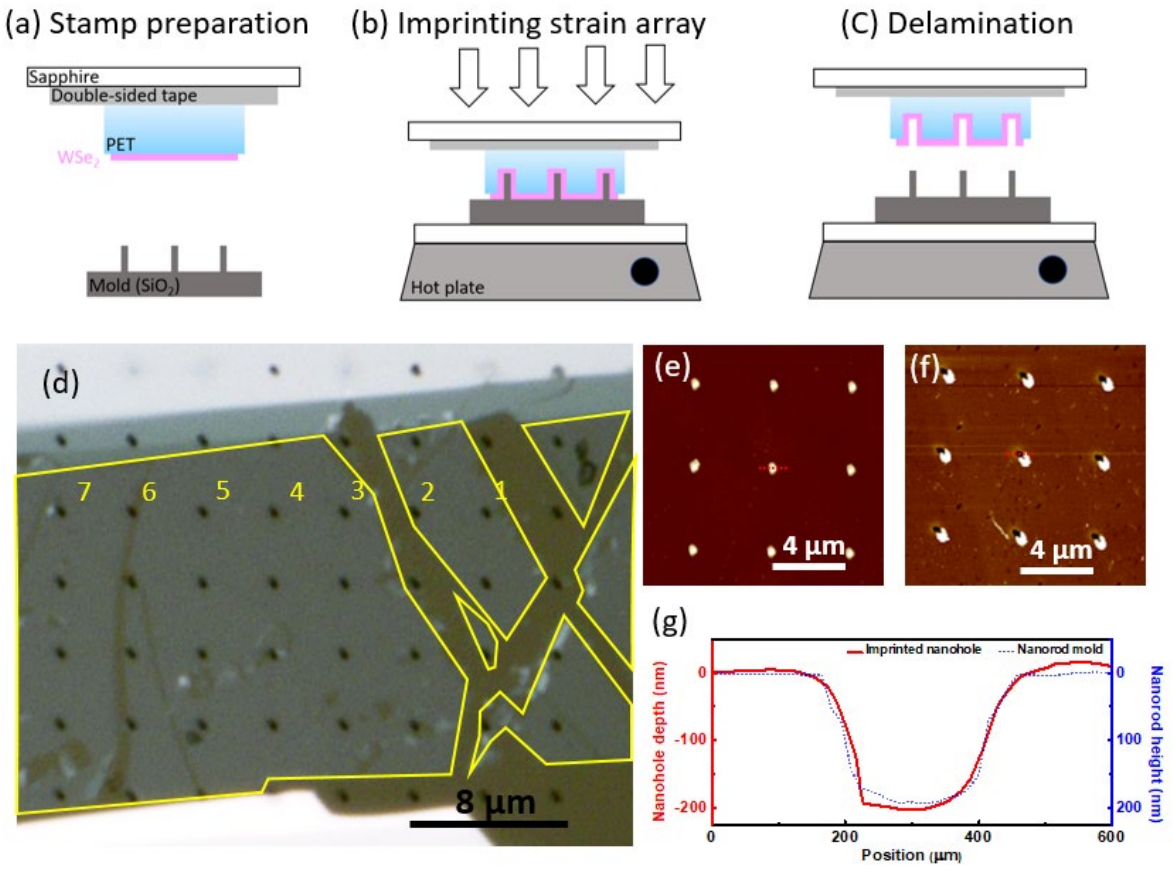

Figure 1. Nanoimprint of WSe_2 on PET. (a)~(c) Schematic of the nano-imprint process. See Methods for more details. (d) Optical microscope image of the imprinted nanostructure array on a WSe_2 ML. (e) AFM top view image of the SiO_2 nanorod mold. (f) AFM image of the imprinted nanohole array on WSe_2, showing a good match with the mold in (e). (g) Height/depth profiles of a nanorod mold and an imprinted nanohole measured by AFM along the red dotted line labeled in (e) and (f).

nanohole. The nanoholes conform well to the morphology of the nanorods, with the same depth of about 200 nm and width of about 200 nm.

To evaluate localized defect activation via the nanoimprint process, we measure the photoluminescence (PL) of the nanoimprinted WSe_2 ML in the spectral region of defect bound

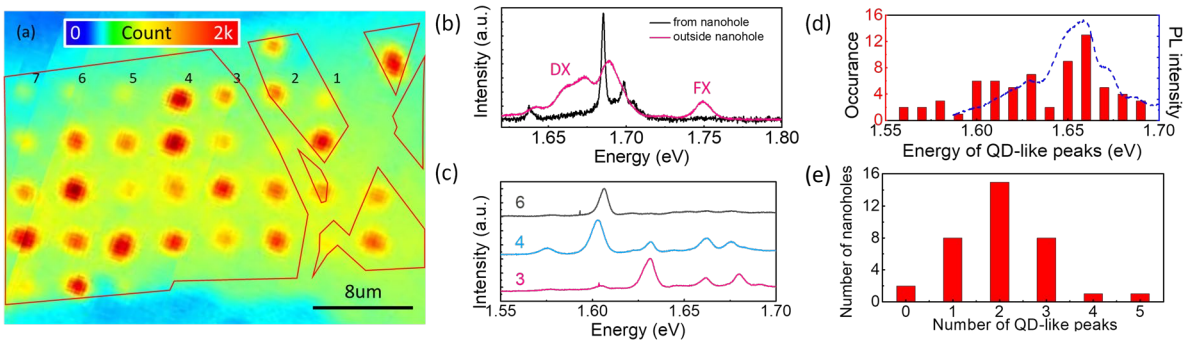

Figure 2. Localized emission from nanoimprinted arrays on a WSe_2 ML. (a) Spatial map of the PL emission from the defect states from a nanoimprinted WSe_2 ML, where the color represents the emission intensity. Localized and enhanced defect state emission is seen at each nanohole site. (b) Comparison of PL spectra from a nanohole site and from outside the nanohole area. The same but relatively high excitation intensity is used to show the free exciton emission. (c) PL spectra at three nanohole sites of different brightness on the WSe_2 ML as labeled in (a), showing different numbers of discrete peaks from localized emitters. (d) A histogram of the peak energy distribution of the localized emission from the nanohole sites imprinted onto theWSe_2 ML, compared with the spectrum of the DX emission measured from the unstrained region (blue dashed line). Both are measured at the same and relatively low excitation intensity. (e) A histogram of the localized emission peaks per nanohole.

excitons, under 532 nm continuous wave (CW) laser excitation. As shown in the wide-field PL microscopy image in Figure 2a, significantly brighter PL intensity is observed from the nanohole sites of the WSe_2 ML, consistent with strain-induced exciton funneling towards the lower energy states.[20] Accompanying the enhancement in emission intensity, the emission spectrum from the nanohole region features discrete and narrowed peaks of 5-10 meV in linewidth (Fig. 2b and 2c),in stark contrast to the broad, 20-50 meV wide, defect exciton (DX) and free exciton (FX) emission from the unstrained region, as we compare in Fig. 2b. The enhanced intensity and narrowed

linewidths of the discrete emission peaks from the nanoholes are consistent with previous reports of single photon emitters localized by strain potentials.[22-24,28,30-32] To confirm that the discrete emission is due to localization of the DX by the strain potential, rather than additional defects introduced through the nanoimprint process, we measure the energy distribution of the localized emitters at all the nanohole sites. As shown in Fig. 2d, it ranges from 1.56eV to 1.69 eV and follows very well the defect-exciton emission of the unstrained WSe_2 ML. These results confirm efficient localization of the defect-excitons by the nanoimprint process.

The different nanoholes exhibit different brightness, which we found to be correlated with the number of localized defect excitons. Shown in Figure 2c are a few representative PL spectra from nanoholes of low (top), high (middle), and moderate (bottom) PL brightness, from nanohole sites as labeled in Figure 2a. Most indented sites show multiple emitters, suggesting that several defect excitons may be localized in each nanohole. The brightest PL corresponds to the greatest number of narrow spectral peaks or localized excitons (Figure 2c middle). The dimmest PL corresponds to a single localized exciton (Figure 2c top). Figure 2e shows the histogram of the emitter number per nanohole site. The average number of emitters per site is about two.

To check the yield of the nanoimprint process, we compare Figure 1d and Figure 2a. The total number of imprinted nanoholes on the ML is 35, as shown in Figure 1d. There are 33 out of the 35 sites exhibiting brightened, narrow emission from localized emitters (Figure 2a). This corresponds to a creation yield of localized emitters of about 94%. In comparison, transferring a ML onto nanostructures typically have a yield below 70%, as the ML is prone to piercing by small nanostructures during the transfer.[24] In the nanoimprint approach, the ML is molded into and remains on the PET substrate, which protects the ML from piercing.

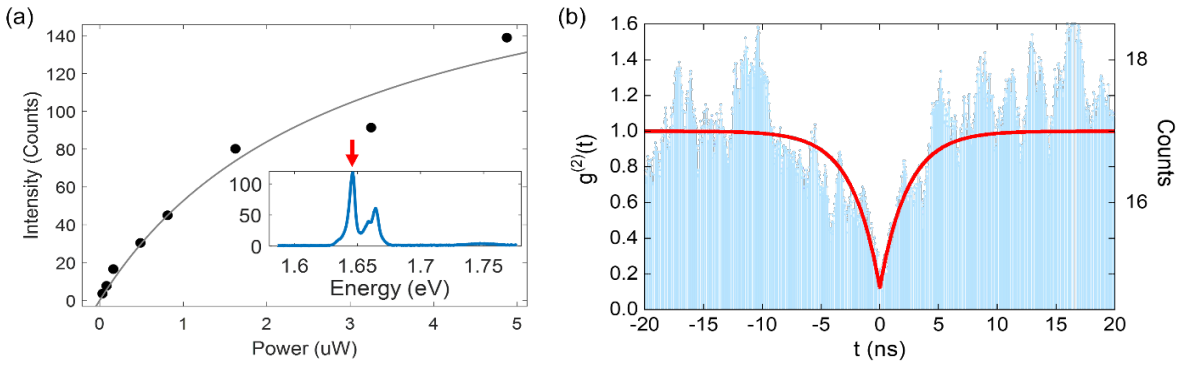

Figure 3. Observation of WSe_2 SPE via nanoimprint activation. (a) The integrated PL counts of the selected PL peak from a nanoimprinted site on the WSe_2 ML, showing saturation behavior with increasing laser power. The solid line is a guide to the eye. Inset is the spectrum of the measured PL without spectral filtering, and the red arrow marks the peak selected by a spectral filter for the measurements in (a) and (b). (b) Second-order correlation function of the emission. The red line is a fit to the data, from which we obtain $g^{(2)}(0) = 0.12$.

To evaluate the single photon property of the localized emitter emission, we measure the power dependence and second order correlation of the emission. As shown in Figure 3a, the emission intensity from one of the localized emitters shows strong saturation with increasing laser excitation power, characteristic of QD emission. We then performed a Hanbury Brown and Twiss type measurement of the photon correlation function $g^{(2)}(\tau)$ for τ the time delay. Figure 3b shows a $g^{(2)}(0) = 0.12$ and $g^{(2)}(\tau)$ decay time of 2.35 ns. The measured photon antibunching confirms the localized emitter at the imprinted site functions as a single photon emitter.

The highest temperature before the emission is quenched is an indication of the strength of the localization potential and efficiency of the single photon emitter. It is also a key factor for applications of SPEs. Reported SPE in un-strained TMDs has been limited to liquid nitrogen

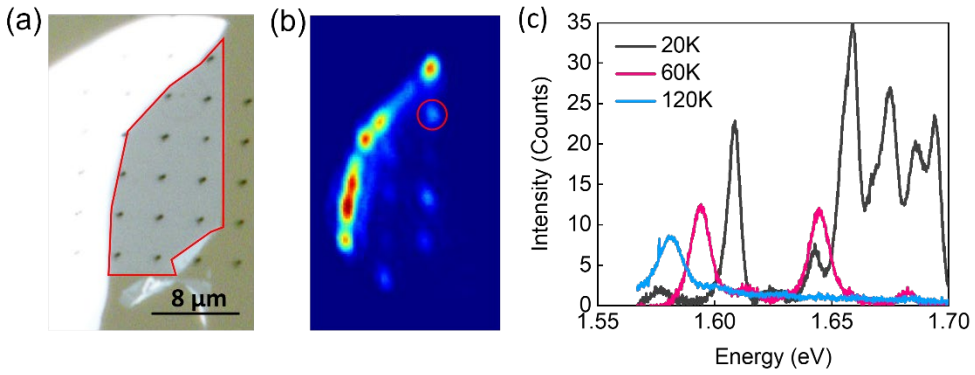

Figure 4. Temperature dependence of localized emitter array created by nanoimprinting. (a) Optical microscope image of the nanoimprinted sample, with the ML region marked by the red outline. (b) Widefield PL image of the nanoimprinted sample at 150 K, showing localized emission from each nanohole site in the ML region. There is also bright defect emission at the left edge of the ML, likely due to strain induced by the nearby bulk. (c) Evolution of the PL spectrum from the emitter circled in (b) with increasing temperature up to 120 K, showing red shift and intensity reduction.

temperature of about 80 K or below, and the defect exciton emission is quenched dramatically at elevated temperatures due to non-radiative recombination.[11,33] To improve the single photon emission, plasmonic cavity has been introduced to boost the emission intensity of the emitters localized by strain by the Purcell effect, and artificial structural defects have been created by e-beam irradiation.[34-36]

To check the high-temperature capability of the nanoimprint approach, we measured the PL mapping of a nanoimprinted ML at different temperatures. Figure 4a and 4b show respectively the optical microscope and wide-field PL images at 150 K. At 150 K, the nano-strained array still features higher emission intensity than that from the un-strained region. From the temperature-

dependent PL spectra shown in Figure 4c, redshift and broadening of the peaks are observed with increasing temperature, which are expected from the reduced bandgap and increased phonon scattering at higher temperatures.[33] The emission intensity of the localized emitters is reduced with increasing temperature. Interestingly, while emitters of higher energies are quenched more rapidly, the lower energy ones bound to deeper defect potentials show a much more gradual decrease in intensity and remain clearly measurable above the background up to 150 K. It suggests the possibility of reducing the number of SPE to one per site by optimizing the operating temperature. To our knowledge, 150 K is the highest operating temperature of position-controlled defect exciton emission without additional enhancement via the Purcell effect or e-Beam irradiation.[34-36] The high operating temperature may be related to the surface passivation of the ML by the PET, which reduces non-radiative channels of the defect exciton.

Lastly, we illustrate the unique rewritable feature of the nanoimprint approach. The imprinted nanohole morphology can be erased by proper pressure and temperature control, as depicted in Figure 5a-b top panel shows the optical microscope image of a nano-imprinted WSe_2 ML before erasure, which is placed in contact with a flat SiO_2 substrate under a gentle press. A clear nanohole array is observed. After increasing the temperature to the glass transition temperature of the PET stamp (63°C), the PET softens and the ML can be flattened under pressure, similar to a wrinkled shirt being ironed. Figure 5b bottom panel shows the optical microscope image of the WSe_2 ML after erasure of the nanoimprints. No nanoholes are observed and the WSe_2 ML becomes flat again. Furthermore, the nanoimprint method also allows rewriting of different patterns on the same ML after an erasure. Figure 5c-d shows an example of rewriting. After a first nanoimprint with a dense nanorod array (Figure 5c), we apply the erasure process to partially remove the nanoimprints with only a faint trace of the sites left, and rewrite onto it a rotated sparse array. As shown in Figure 5d,

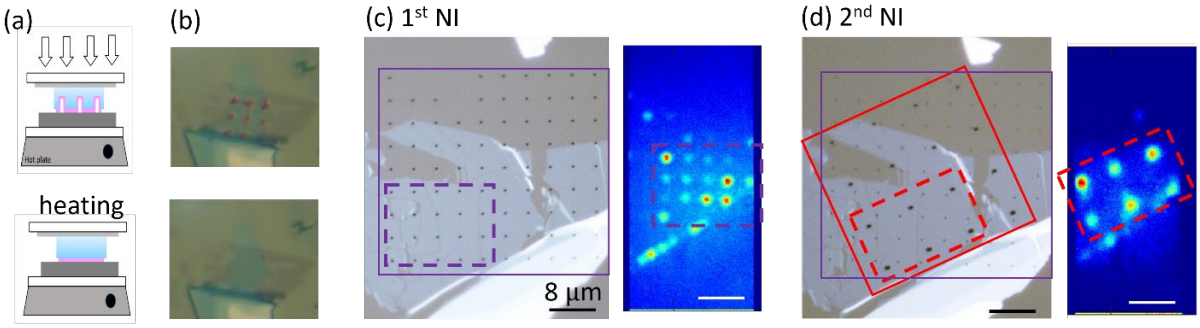

Figure 5. Erasure and rewriting of strained nanohole arrays. (a) Schematic of the erasing process. (b) Optical microscope images of a nanoimprinted sample before (top) and after (bottom) erasure. (c) Optical microscope (left) and spectrally filtered PL (right) images of a ML after the first nanoimprinting, showing localized emission from the imprinted sites. (d) Comparison with (c) after erasure and reprint on the same ML. Traces from the first dense-array nanoimprint were left for references, while localized emission is observed only from the rotated sparse array created by the second nanoimprint. In (c-d), the purple and red outlines mark the first and second nanoimprinted arrays, respectively. The dashed outlines mark the same ML region in the microscope and PL images. All scale bars are 8 μm wide.

the new sparse array is imprinted onto the ML, creating localized emission from the imprinted sites, while no localized emission is observed from dense array sites of the first nanoimprint. The erasure and rewrite capabilities not only allow the reuse of MLs but also, and error-correction and improved spatial positioning in creating SPE arrays, which can be especially important such as when the SPEs need to be precisely positioned to couple with waveguides or photonic-crystal cavities.

In summary, we demonstrate nanoimprinting as a flexible, fast, controlled method to create strain induced localized emitter arrays in 2D materials. The imprinted nanoholes conform well to

the morphology of the nano-mold. Bright, discrete defect-exciton emission from the imprinted sites suggests efficient exciton funneling via nano-scale strain engineering. Single-photon emission from the imprinted sites is verified by photon anti-bunching. The high yield of localized emitters and high operating temperature of the emission suggest both effectiveness of the nanoimprint method in creating localized emitters and the potential of creating SPE in TMDs under more practical conditions. Furthermore, the method allows erasing and re-writing of SPE arrays, which will facilitate applications that need high spatial precision and controllability. The imprinted nanohole morphology remains protected in polyester substrate and thus can be readily integrated with additional photonic structure, such as waveguides and nanocavities, which are often critical for applications of SPEs.[32] The emission linewidth of the localized excitons is relatively broad at present, which may be improved by encapsulation by hexagon boron nitride and further optimization of the nanoimprinting procedure.[37] The method should be applicable to nanoscale strain engineering of a wide range of 2D material systems, including hexagon boron nitride, atomically thin heterostructures, and wafer-scale grown 2D materials.[38-40] With further improvements in material qualities and fabrication procedures, nanoimprinting applied to 2D materials may provide a new pathway to scalable quantum photonic circuits.

Methods

Nanoimprint procedure. The nanorod array template, which serves as an imprinting mold, is fabricated on a SiO_2-capped Si substrate by electron beam lithography and dry etching process. The nanorods have a height of 200 nm, diameter of 200 nm, and rod-to-rod separation of 4 μm. To perform nanoimprinting, first, the WSe_2 ML is exfoliated from the bulk crystal and transfer onto a Si substrate with a 285 nm SiO_2 capping layer by a polydimethylsiloxane (PDMS) stamp.

Then the WSe_2 is pick up by a polyester (PET) stamp which is adhered to a sapphire substrate by a transparent double-sided tape. An optical microscope is used for monitoring the indenting process. Both the mold and the PET stamp with the ML are mounted on three-axis translation stages for precise positioning and indenting. As the stamp is transparent, one can see the nanorod array through it, thus allowing precise alignment between the monolayer flake and the nanorods. The stamp is pressed gently on the mold and the stage of the mold is heated up to 63°C, which is the glass transition temperature of the PET, to help the mold contacting with the stamp. After the mold and the stamp come into total contact, the mold is cooled down to the room temperature. Then the stamp is delaminated from the mold.

Optical measurement. All optical measurements reported herein were performed via a home-built confocal microscope with an objective lens with a numerical aperture of NA = 0.42. The sample was cooled to 5 K using a Montana Instruments Fusion 2 cryostat. All spectra were acquired with Princeton Instruments spectrometer with a measured spectral resolution of 0.3 nm and a cooled charge-coupled camera. A free-space Hanbury Brown and Twist interferometer was utilized for characterizing second-order photon correlation function. The photon counting was performed using avalanche photodiodes (APDs). A 150 μm pinhole and two bandpass filters were utilized to spatially and spectrally select only one quantum emitter.

AUTHOR INFORMATION

Corresponding Author

*E-mail: dengh@umich.edu

Author Contributions

Y.Y.L. fabricated the MLs, developed nanoimprinting, performed optical measurements and data analysis. P.H.C. and C.A.C. fabricated the nanomolds and performed AFM measurements. Y.S.L. and H.D. supervised the project. Y.Y.L. and H.D. wrote the paper with inputs from other authors. All authors discussed the results, data analysis and the paper.

Notes

The authors declare that they have no competing financial interests.

Data Availability

Data are available on request from the authors.

ACKNOWLEDGMENT

Y.L. and H.D. acknowledge the support by the Air Force Office of Scientific Research under Awards FA2386-21-1-4066, the Army Research Office under Awards W911NF-17-1-0312 and the National Science Foundation under Awards DMR-2132470. Y.L. and Y.H.L. acknowledge support from Ministry of Science and Technology (MoST 109-2124-M-007-001-MY3; 107-2923-M-007-002-MY3). Y.L. would like to thank Dr. L. Zhang and Ms. E. Paik at University of Michigan for their technical support and fruitful discussions.

Funding Sources

1. Air Force Office of Scientific Research under Awards FA2386-21-1-4066
2. Army Research Office under Awards W911NF-17-1-0312
3. National Science Foundation under Awards DMR-2132470

4. Ministry of Science and Technology of Taiwan under MoST 109-2124-M-007-001-MY3; 107-2923-M-007-002-MY3

REFERENCES

1. Aharonovich, I.; Englund, D.; Toth, M. Solid-state single-photon emitters. *Nat. Photonics* **2016**, 10 (10), 631-641. DOI: 10.1038/Nphoton.2016.186.

2. Santori, C.; Pelton, M.; Solomon, G.; Dale, Y.; Yamamoto, Y. Triggered Single Photons from a Quantum Dot. *Phys. Rev. Lett.* **2001**, 86 (8), 1502-1505. DOI: 10.1103/PhysRevLett.86.1502.

3. Lee, L. K.; Zhang, L.; Deng, H.; Ku, P. C. Room-temperature quantum-dot-like luminescence from site-controlled InGaN quantum disks. *Appl. Phys. Lett.* **2011**, 99 (26), 263105. DOI: 10.1063/1.3672441.

4. Ma, X.; Hartmann, N. F.; Baldwin, J. K. S.; Doorn, S. K.; Htoon, H. Room-temperature single-photon generation from solitary dopants of carbon nanotubes. *Nat. Nanotechnol.* **2015**, 10 (8), 671-675. DOI: 10.1038/nnano.2015.136.

5. Kurtsiefer, C.; Mayer, S.; Zarda, P.; Weinfurter, H. Stable Solid-State Source of Single Photons. *Phys. Rev. Lett.* **2000**, 85 (2), 290-293. DOI: 10.1103/PhysRevLett.85.290.

6. Michler, P.; Imamoglu, A.; Mason, M. D.; Carson, P. J.; Strouse, G. F.; Buratto, S. K. Quantum correlation among photons from a single quantum dot at room temperature. *Nature* **2000**, 406 (6799), 968-970. DOI: 10.1038/35023100.

7. Park, Y.-S.; Guo, S.; Makarov, N. S.; Klimov, V. I. Room Temperature Single-Photon Emission from Individual Perovskite Quantum Dots. *ACS Nano* **2015**, 9 (10), 10386-10393. DOI: 10.1021/acsnano.5b04584.

8. Srivastava, A.; Sidler, M.; Allain, A. V.; Lembke, D. S.; Kis, A.; Imamoğlu, A. Optically active quantum dots in monolayer WSe_2. *Nat. Nanotechnol.* **2015**, 10 (6), 491-496. DOI: 10.1038/nnano.2015.60.

9. Koperski, M.; Nogajewski, K.; Arora, A.; Cherkez, V.; Mallet, P.; Veuillen, J. Y.; Marcus, J.; Kossacki, P.; Potemski, M. Single photon emitters in exfoliated WSe_2 structures. *Nat. Nanotechnol.* **2015**, 10 (6), 503-506. DOI: 10.1038/nnano.2015.67.

10. Chakraborty, C.; Kinnischtzke, L.; Goodfellow, K. M.; Beams, R.; Vamivakas, A. N. Voltage-controlled quantum light from an atomically thin semiconductor. *Nat. Nanotechnol.* **2015**, 10 (6), 507-511. DOI: 10.1038/nnano.2015.79.

11. He, Y.-M.; Clark, G.; Schaibley, J. R.; He, Y.; Chen, M.-C.; Wei, Y.-J.; Ding, X.; Zhang, Q.; Yao, W.; Xu, X.; Lu, C.-Y.; Pan, J.-W. Single quantum emitters in monolayer semiconductors. *Nat. Nanotechnol.* **2015**, 10(6), 497-502. DOI: 10.1038/nnano.2015.75.

12. Palacios-Berraquero, C.; Barbone, M.; Kara, D. M.; Chen, X.; Goykhman, I.; Yoon, D.; Ott, A. K.; Beitner, J.; Watanabe, K.; Taniguchi, T.; Ferrari, A. C.; Atatüre, M. Atomically thin quantum light-emitting diodes. *Nat. Commun.* **2016**, 7(1), 12978. DOI: 10.1038/ncomms12978.

13. Tonndorf, P.; Schwarz, S.; Kern, J.; Niehues, I.; Del Pozo-Zamudio, O.; Dmitriev, A. I.; Bakhtinov, A. P.; Borisenko, D. N.; Kolesnikov, N. N.; Tartakovskii, A. I.; Michaelis de

Vasconcellos, S.; Bratschitsch, R. Single-photon emitters in GaSe. *2D Mater.* **2017**, 4 (2), 021010. DOI: 10.1088/2053-1583/aa525b.

14. Tran, T. T.; Bray, K.; Ford, M. J.; Toth, M.; Aharonovich, I. Quantum emission from hexagonal boron nitride monolayers. *Nat. Nanotechnol.* **2016**, 11(1), 37-41. DOI: 10.1038/nnano.2015.242.

15. Ren, S.; Tan, Q.; Zhang, J. Review on the quantum emitters in two-dimensional materials. *J. Semicond.* **2019**, 40 (7), 071903. DOI: 10.1088/1674-4926/40/7/071903.

16. Kumar, S.; Kaczmarczyk, A.; Gerardot, B. D. Strain-Induced Spatial and Spectral Isolation of Quantum Emitters in Mono- and Bilayer WSe_2. *Nano Lett.* **2015**, 15(11), 7567-7573. DOI: 10.1021/acs.nanolett.5b03312.

17. Kern, J.; Niehues, I.; Tonndorf, P.; Schmidt, R.; Wigger, D.; Schneider, R.; Stiehm, T.; Michaelis de Vasconcellos, S.; Reiter, D. E.; Kuhn, T.; Bratschitsch, R. Nanoscale Positioning of Single-Photon Emitters in Atomically Thin WSe_2. *Adv. Mater.* **2016**, 28(33), 7101-7105. DOI: 10.1002/adma.201600560

18. Yu, L.; Deng, M.; Zhang, J. L.; Borghardt, S.; Kardynal, B.; Vučković, J.; Heinz, T. F. Site-Controlled Quantum Emitters in Monolayer $MoSe_2$. *Nano Lett*. **2021**, 21(6), 2376-2381. DOI: 10.1021/acs.nanolett.0c04282

19. Palacios-Berraquero, C.; Kara, D. M.; Montblanch, A. R. P.; Barbone, M.; Latawiec, P.; Yoon, D.; Ott, A. K.; Loncar, M.; Ferrari, A. C.; Atatüre, M. Large-scale quantum-emitter arrays in atomically thin semiconductors. *Nat. Commun.* **2017**, 8(1), 15093. DOI: 10.1038/ncomms15093.

20. Branny, A.; Kumar, S.; Proux, R.; Gerardot, B. D. Deterministic strain-induced arrays of quantum emitters in a two-dimensional semiconductor. *Nat. Commun.* **2017**, 8(1), 15053. DOI: 10.1038/ncomms15053.

21. Luo, Y.; Shepard, G. D.; Ardelean, J. V.; Rhodes, D. A.; Kim, B.; Barmak, K.; Hone, J. C.; Strauf, S. Deterministic coupling of site-controlled quantum emitters in monolayer WSe_2 to plasmonic nanocavities. *Nat. Nanotechnol.* **2018**, 13(12), 1137-1142. DOI: 10.1038/s41565-018-0275-z.

22. Cai, T.; Kim, J.-H.; Yang, Z.; Dutta, S.; Aghaeimeibodi, S.; Waks, E. Radiative Enhancement of Single Quantum Emitters in WSe_2 Monolayers Using Site-Controlled Metallic Nanopillars. *ACS Photonics* **2018**, 5, 3466–3471, DOI: 10.1021/acsphotonics.8b00580.

23. Tripathi, L. N.; Iff, O.; Betzold, S.; Dusanowski, Ł.; Emmerling, M.; Moon, K.; Lee, Y. J.; Kwon, S.-H.; Höfling, S.; Schneider, C. Spontaneous emission enhancement in strain-induced WSe_2 monolayer-based quantum light sources on metallic surfaces. *ACS Photonics* **2018**, 5, 1919–1926, DOI: 10.1021/acsphotonics.7b01053.

24. Wang, W.; Ma, X. Strain-Induced Trapping of Indirect Excitons in $MoSe_2/WSe_2$ Heterostructures. *ACS Photonics* **2020**, 7, 2460–2467, DOI: 10.1021/acsphotonics.0c00567.

25. Iff, O.; Lundt, N.; Betzold, S.; Tripathi, L. N.; Emmerling, M.; Tongay, S.; Lee, Y. J.; Kwon, S.-H.; Höfling, S.; Schneider, C. Deterministic coupling of quantum emitters in WSe_2 monolayers to plasmonic nanocavities. *Opt. Express* **2018**, 26(20), 25944-25951. DOI: 10.1364/OE.26.025944.

26. Kim, H.; Moon, J. S.; Noh, G.; Lee, J.; Kim, J.-H. Position and Frequency Control of Strain-Induced Quantum Emitters in WSe_2 Monolayers. *Nano Lett.* **2019**, 19(10), 7534-7539. DOI: 10.1021/acs.nanolett.9b03421.

27. Mukherjee, A.; Chakraborty, C.; Qiu, L.; Vamivakas, A. N. Electric field tuning of strain-induced quantum emitters in WSe_2. *AIP Adv*. **2020**, 10(7), 075310. DOI: 10.1063/5.0010395.

28. Rosenberger, M. R.; Dass, C. K.; Chuang, H.-J.; Sivaram, S. V.; McCreary, K. M.; Hendrickson, J. R.; Jonker, B. T. Quantum Calligraphy: Writing Single-Photon Emitters in a Two-Dimensional Materials Platform. *ACS Nano* **2019**, 13(1), 904-912. DOI: 10.1021/acsnano.8b08730.

29. Chou, S. Y.; Krauss, P. R.; Renstrom, P. J. Imprint Lithography with 25-Nanometer Resolution. *Science* **1996**, 272(5258), 85-87. DOI: doi:10.1126/science.272.5258.85.

30. Tonndorf, P.; Schmidt, R.; Schneider, R.; Kern, J.; Buscema, M.; Steele, G. A.; Castellanos-Gomez, A.; van der Zant, H. S. J.; Michaelis de Vasconcellos, S.; Bratschitsch, R. Single-Photon Emission from Localized Excitons in an Atomically Thin Semiconductor. *Optica* **2015**, 2, 347–352, DOI: 10.1364/OPTICA.2.000347

31. Blauth, M.; Jürgensen, M.; Vest, G.; Hartwig, O.; Prechtl, M.; Cerne, J.; Finley, J. J.; Kaniber, M. Coupling Single Photons from Discrete Quantum Emitters in WSe2 to Lithographically Defined Plasmonic Slot Waveguides. *Nano Lett*. **2018**, 18, 6812–6819, DOI: 10.1021/acs.nanolett.8b02687

32. Peyskens, F.; Chakraborty, C.; Muneeb, M.; Van Thourhout, D.; Englund, D. Integration of single photon emitters in 2D layered materials with a silicon nitride photonic chip. *Nat. Commun.* **2019**, 10(1), 4435. DOI: 10.1038/s41467-019-12421-0.

33. He, Y.-M.; Höfling, S.; Schneider, C. Phonon induced line broadening and population of the dark exciton in a deeply trapped localized emitter in monolayer WSe_2. *Opt. Express* **2016**, 24(8), 8066-8073. DOI: 10.1364/OE.24.008066.

34. Luo, Y.; Liu, N.; Li, X.; Hone, J. C.; Strauf, S. Single photon emission in WSe_2 up 160 K by quantum yield control. *2D Mater*. **2019**, 6(3), 035017. DOI: 10.1088/2053-1583/ab15fe.

35. Edelberg, D.; Rhodes, D.; Kerelsky, A.; Kim, B.; Wang, J.; Zangiabadi, A.; Kim, C.; Abhinandan, A.; Ardelean, J.; Scully, M.; Scullion, D.; Embon, L.; Zu, R.; Santos, E. J. G.; Balicas, L.; Marianetti, C.; Barmak, K.; Zhu, X.; Hone, J.; Pasupathy, A. N. Approaching the Intrinsic Limit in Transition Metal Diselenides via Point Defect Control. *Nano Lett.* **2019**, 19(7), 4371-4379. DOI: 10.1021/acs.nanolett.9b00985

36. Parto, K.; Azzam, S. I.; Banerjee, K.; Moody, G. Defect and strain engineering of monolayer WSe_2 enables site-controlled single-photon emission up to 150 K. . *Nat. Commun.* **2021**, 12(1), 3585. DOI: 10.1038/s41467-021-23709-5.

37. Wierzbowski, J.; Klein, J.; Sigger, F.; Straubinger, C.; Kremser, M.; Taniguchi, T.; Watanabe, K.; Wurstbauer, U.; Holleitner, A. W.; Kaniber, M.; Müller, K.; Finley, J. Direct exciton emission from atomically thin transition metal dichalcogenide heterostructures near the lifetime limit. *Sci. Rep.* **2017**, 7, 12383, DOI: 10.1038/s41598-017-09739-4

38. Shim, J.; Bae, S.-H.; Kong, W.; Lee, D.; Qiao, K.; Nezich, D.; Park, Y. J.; Zhao, R.; Sundaram, S.; Li, X.; Yeon, H.; Choi, C.; Kum, H.; Yue, R.; Zhou, G.; Ou, Y.; Lee, K.; Moodera, J.; Zhao, X.; Ahn, J.-H.; Hinkle, C.; Ougazzaden, A.; Kim, J. Controlled crack propagation for atomic precision handling of wafer-scale two-dimensional materials. *Science* **2018**, 362(6415), 665-670. DOI: doi:10.1126/science.aat8126.

39. Kang, K.; Lee, K.-H.; Han, Y.; Gao, H.; Xie, S.; Muller, D. A.; Park, J. Layer-by-layer assembly of two-dimensional materials into wafer-scale heterostructures. *Nature* **2017**, 550 (7675), 229-233. DOI: 10.1038/nature23905.

40. So, J.-P.; Kim, H.-R.; Baek, H.; Jeong, K.-Y.; Lee, H.-C.; Huh, W.; Kim, Y. S.; Watanabe, K.; Taniguchi, T.; Kim, J.; Lee, C.-H.; Park, H.-G. Electrically driven strain-induced deterministic single-photon emitters in a van der Waals heterostructure. *Sci. Adv.* **2021**, 7(43), eabj3176. DOI: doi:10.1126/sciadv.abj3176.

For Table of Contents Use Only

Single Photon Emission from Rewritable Nanoimprinted Localized Emitter Arrays in Atomically Thin Crystals

Ying-Yu Lai, Po-Han Chen, Chun-An Chen, Yi-Hsien Lee, and Hui Deng

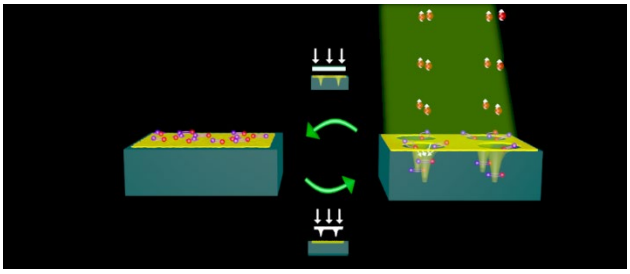

Single photon emission from reversibly nanoimprinted nanohole arrays.